Diamond anvil cell radial x-ray diffraction program at the National Synchrotron Light Source

2006 J. Phys.: Condens. Matter 18 S1091

(http://iopscience.iop.org/0953-8984/18/25/S16)

INSTITUTE OF PHYSICS PUBLISHING JOURNAL OF PHYSICS: CONDENSED MATTER

J. Phys.: Condens. Matter **18** (2006) S1091–S1096 doi:10.1088/0953-8984/18/25/S16

Diamond anvil cell radial x-ray diffraction program at the National Synchrotron Light Source

J Z Hu[1], H K Mao[2], J F Shu[2], Q Z Guo[1] and H Z Liu[2]

[1] X17 of NSLS, CARS, University of Chicago, Upton, NY 11973, USA
[2] Geophysical Laboratory, Carnegie Institution of Washington, Washington, DC 20015, USA

E-mail: jzhu@bnl.gov

Received 21 February 2006, in final form 2 May 2006
Published 8 June 2006
Online at stacks.iop.org/JPhysCM/18/S1091

Abstract

During the past decade, the radial x-ray diffraction method using a diamond anvil cell (DAC) has been developed at the X17C beamline of the National Synchrotron Light Source. The detailed experimental procedure used with energy dispersive x-ray diffraction is described. The advantages and limitations of using the energy dispersive method for DAC radial diffraction studies are also discussed. The results for FeO at 135 GPa and other radial diffraction experiments performed at X17C are discussed in this report.

1. Introduction

X17C, a side branch of the high-energy, high-intensity superconducting-wiggler x-ray beam line X17 of the National Synchrotron Light Source (NSLS), at Brookhaven National Laboratory, is dedicated to DAC high-pressure research. With a five-pole, 4.2 T superconducting wiggler, the brightness and brilliance of X17C in the energy region from 5 to 80 keV is 5–10 times higher than that of bending magnet beam lines at the Advanced Photon Sources (APS) [1] as shown in figure 1. Such x-radiation is especially effective for penetrating diamond windows and measuring diffraction of minute samples at ultrahigh pressures.

2. Experimental set-up

The energy dispersive x-ray diffraction (ED-XRD) system at X17C is shown in figure 2. The primary slit system consists of a horizontal slit and a vertical slit which are made of four 10 mm thick tungsten blocks. The motorized slits define the horizontal and vertical positions and sizes of the incident x-ray beam. A pair of 100 mm length Kirkpatrick–Baez (KB) mirrors consisting of Si crystals coated with Pt is used for focusing the white x-ray beam at a glancing angle of approximately 1 mrad [2]. The best focusing is obtained using a 50 μm $\times$ 50 μm incident beam size which is focused to 10 μm (horizontal) $\times$ 6 μm (vertical). Between the KB mirrors and

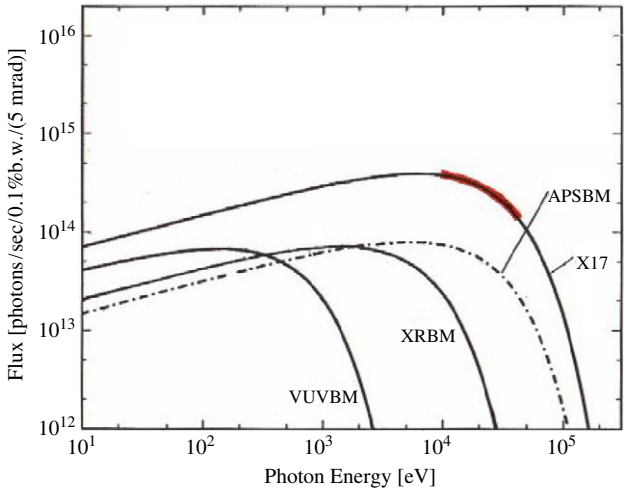

Figure 1. Synchrotron beam flux versus energy at X17C. NSLS ring current: 300 mA, Wiggler magnetic field $B = 4.2$ T; APS BM: 100 mA.

(This figure is in colour only in the electronic version)

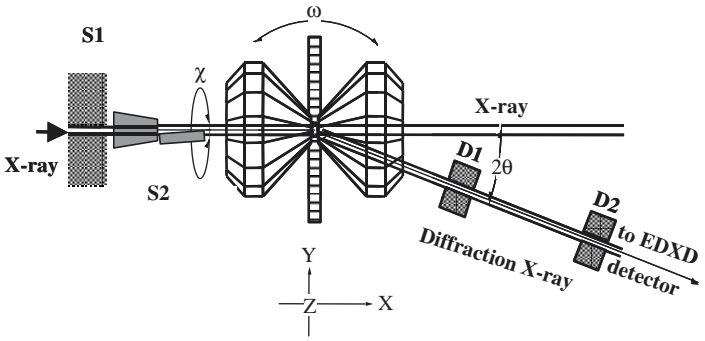

Figure 2. A schematic diagram of ED-XRD at X17C, in which S1: primary beam slit; S2: KB mirrors; D1, D2: receiving slits.

the sample, a cleanup slit of size 40 μm $\times$ 40 μm is used for reducing the low-intensity tails of the focused beam. The sample in the DAC is located at the rotation centre of a goniometer. The system has motorized ω and χ rotation stages and linear translation stages in the X, Y, and Z directions. A Canberra intrinsic Ge solid detector (model GL0055PS) on the 2θ arm collects the diffraction signal after it passes through two receiving slits, D1 and D2. The receiving slit D1 provides spatial resolution and D2 determines the 2θ angular resolution. The D1 slit size ranges from 25 to 100 μm in the horizontal direction and 300–500 μm in the vertical direction; the D2 slit size is 200 μm in the horizontal direction and 4–6 mm in the vertical direction. D1 is located about 20–25 mm from the sample and D2 is about 220–250 mm from the sample. The detector energy resolution is 220 eV at 8.04 keV, and about 360 eV at 59.54 keV.

The combination of microscopic incident beam and finely collimated diffracted beam at X17C provides excellent spatial resolution for separating the diffraction signals of the sample from those of the high-strength beryllium gasket in the DAC [3]. Figure 3 shows the geometry of a radial x-ray diffraction (RXD) experiment. The x-ray beam passes through

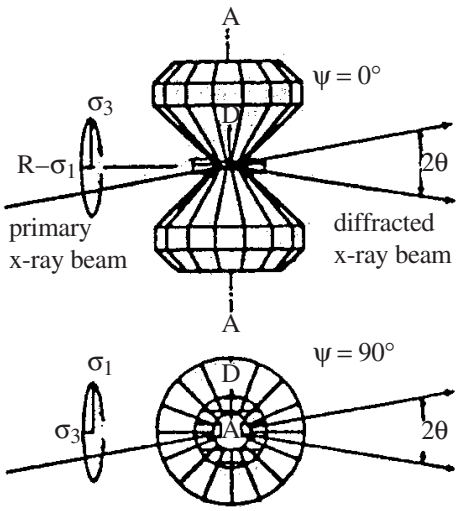

Figure 3. Radial x-ray diffraction geometry.

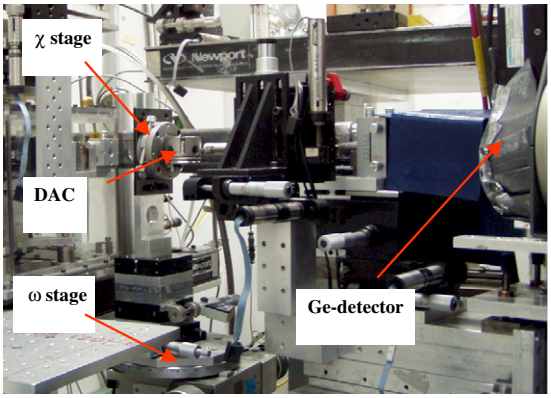

Figure 4. Radial x-ray diffraction setup for $\psi = 90°$ at X17C. Ge detector at fixed 2θ angle.

the beryllium gasket in the radial direction and probes the lattice strains of a polycrystalline specimen subjected to a uniaxial stress. The DAC is mounted on a χ rotation stage, in which the uniaxial compression direction of the DAC is perpendicular to the rotation axis of χ that bisects the 2θ angle between the incident and diffracted x-ray beams. The angle ψ between the diffraction vector and the DAC axis is varied as the DAC rotates around the χ axis. Figure 4 shows a photograph of the RXD setup for the $\psi = 90°$ geometry at X17C. Before RXD experiments, the sample is centred in the χ rotation stage using an off-line, motor-driven χ-rotation alignment system. Then the χ rotation stage containing the DAC is mounted on the goniometer. At $\omega = 90°$, $\chi = 0°$, the DAC is in conventional axial ED-XRD geometry, as shown in figure 2. The sample is then aligned to the rotation axis of the ω stage following the normal alignment procedure. First, sample x, y, and z positions are optically aligned with a microscope. Then the sample centre position is defined according to the profile of absorption intensity of sample measured from an air ionization chamber located in the downstream x-ray beam path. When ω is rotated to 0°, the sample is in the correct position for the radial diffraction geometry where $\chi = 0°$, and $\psi \approx 0°$, as shown in figure 3. For different ψ angles, the sample centre is verified by scanning the horizontal and vertical translation stages across the incident x-ray beam and measuring sample absorption with the ion chamber. To avoid

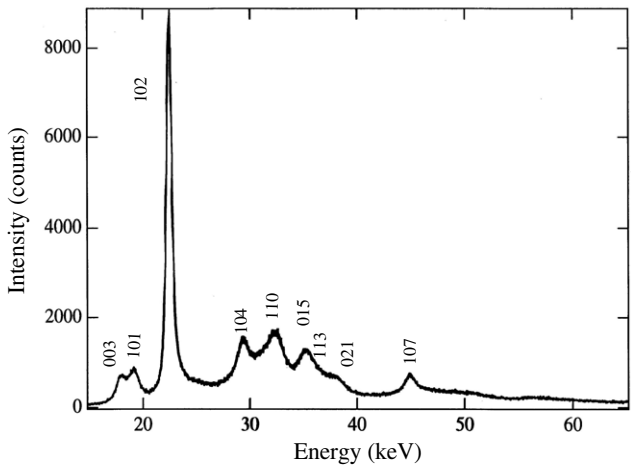

Figure 5. ED-XRD spectrum of rhombohedral phase FeO at 135 GPa and $\psi = 90°$, $2\theta = 17°$.

diffraction peaks from the beryllium gasket, a 10 μm $\times$ 6 μm focused incident beam and a 30 μm (width) receiving slit (D1) were used to reduce the sampled area, i.e., intersection of incident and diffraction beams, to a 10 μm $\times$ 30 μm lozenge. A 0.2 mm $\times$ 6 mm secondary receiving slit (D2) was used for achieving sufficient angular resolution.

Compared to the angle-dispersive x-ray diffraction (AD-XRD) method using a two-dimensional detector, the ED-XRD using a point detector has gradually been losing ground in the high-pressure synchrotron community since the mid-1990s because of its low resolution and its access to only a small part of the Debye–Scherrer cone [4]. However, for RXD, ED has the unique geometrical advantage that for each diffraction pattern, ED-XRD measures the same strain direction ψ for all diffraction peaks, while AD-XRD measures different ψ depending upon the θ and χ angles. In addition, the ED-XRD method has the advantage of selecting a tiny diffraction intersection lozenge zone to avoid the diffraction peaks from gasket materials, such as the strong diffraction peaks from a Be gasket. An example of an RXD spectrum showing a rhombohedral FeO ED pattern at 135 GPa without a beryllium gasket signal is presented in figure 5.

3. Applications

Using the RXD method, experiments under deviatoric stress can provide information about strength, elasticity and preferred orientation of polycrystalline materials exceeding megabar pressures [5–7]. In RXD, the d-spacing of a polycrystalline sample under uniaxial stress varies linearly with $(1 - 3\cos^2\psi)$:

$$d_{(hkl)} = d_{p(hkl)}[(1 - 3\cos^2\psi)Q_{(hkl)} + 1] \tag{1}$$

where $d_{p(hkl)}$ is the d-spacing under hydrostatic pressure, and $Q_{(hkl)}$ is a function of the single-crystal elasticity tensor [5, 6]. Figure 6 shows how the d-spacings of the first three diffraction peaks of the rhombohedral-phase FeO at 135 GPa vary with $(1 - 3\cos^2\psi)$.

Single-crystal elasticity tensors (C_{ij}) of polycrystalline materials can be derived from RXD data with assumptions of α between isostrain ($\alpha = 0$) and isostress ($\alpha = 1$) conditions. For example, the elasticity tensors for hexagonal-close-packed (hcp) Fe were estimated from RXD data to 211 GPa [3, 7]. In that study, a relatively large shear elastic anisotropy as given by the ratio C_{44}/C_{66} was observed which was bigger than the results from first-principles

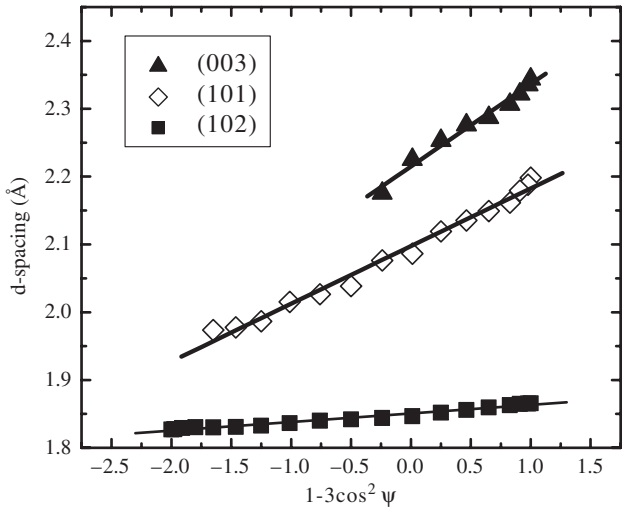

Figure 6. d-spacings of FeO at 135 GPa versus $(1 - 3\cos^2\psi)$, in which ψ varies from 0° to 90°.

calculations [8–10]. The RXD data of Fe may reflect stress variation owing to preferred slip systems [11], and a similar anomalous anisotropy for the hcp metal Re was also observed [12]. This may suggest that the α value could be mathematically bigger than 1 if estimates are based on the less elastic anisotropy model. However, $\alpha = 0.5$ or 1 was generally used in the data analysis process in various papers [3, 5–7]. This reflects the need for a more advanced analytical model. The effects of texture [13, 14] and plastic deformation [15] on the elasticity measurement have also been documented. A recent RXD experimental study up to 30 GPa to determine the single-crystal elastic moduli of hcp Fe yielded comparable C_{44} and C_{66} values [16].

From the texture pattern of deformed materials, it is possible to infer active deformation mechanisms by comparing experiments with corresponding polycrystal plasticity simulations. One excellent example was the RXD study of hcp Fe at 220 GPa [17]. Iron crystals displayed strong preferred orientation, with c-axes parallel to the axes of the DAC. A large plastic strain of 50%–100% was observed, and it was inferred that basal slip was the active deformation mechanism in hcp Fe, probably in combination with other systems. Even if prismatic slip was favoured, basal slip became dominant as preferred orientation developed [17].

From RXD data, we can determine the differential stress of material under uniaxial compression. For example, the differential stress of an OH-bearing (hydrous) ringwoodite increases from 2.9 to 4.5 GPa over the pressure range 6.7–13.2 GPa at room temperature [18]. This result suggests a significant water weakening effect when compared with results from similar experiments on the anhydrous counterpart [19].

From RXD data, we can also derive unbiased bulk modulus and other P–V equation-of-state parameters comparable to those obtained from hydrostatic experiments. Conventional axial XRD measures d-spacings at $\psi = 90° \pm 10°$ that are systematically larger than the unbiased d_p at the pressure P. Based on equation (1), we can determine the unbiased d_p value at a specific angle of $\psi = 57.4°$ [20] where $3\cos^2\psi = 1$ and $d = d_P$. More precisely, we can also obtain d_p from fitting the d–ψ data to equation (1). The resultant P–d_p data would have eliminated most of the nonhydrostatic components and would be close to data from hydrostatic experiments. For example, the RXD data of B_6O up to 65.3 GPa yielded a bulk modulus $K_0 = 270 \pm 12$ GPa and its pressure derivative $K_0' = 1.8 \pm 0.3$ [21].

4. Conclusions

Using ED-XRD at X17C, elastic and strength properties of many materials under uniaxial compression and high pressures have been obtained. The results provide rich information about seismic anisotropy of materials that are expected to be present in the Earth's deep interior, including the inner core material iron [3, 5–7, 17]. This technique has been extended by various X17C general users to studies of other highly strained minerals, metals, and superhard materials, including ringwoodite [18, 19], pyrite [22], silica [23], magnesium oxide [24], gold [12, 25], rhenium [12], molybdenum [25], platinum [26], boron suboxide (B_6O) [21], and γ-Si_3N_4 [27].

In summary, radial x-ray diffraction for high-pressure DAC experiments in energy dispersive mode is well developed at the X17C beamline of NSLS, and has become one of the routine operation settings for general users of the high-pressure research community. In addition to Earth science applications, this technique has also been widely used in materials science, condensed matter physics, and solid state chemistry.

Acknowledgments

The authors thank Tom Duffy for helpful discussions. This work is supported by NSF COMPRES EAR01-35554, and by US-DOE contract DE-AC02-10886 to NSLS.

References

[1] Zhong Z 2006 personal communication
[2] Eng P J, Rivers M, Yang B X and Schildkamp W 1995 Micro-focusing 4 keV to 65 keV x-rays with Bent Kirkpatrick–Baez mirrors *X-ray Microbeam Technology and Applications* (*Proc.* vol 2516) ed W Yun, p 41
[3] Mao H K, Hemley R J and Mao A L 1997 *Advances in High Pressure Research in Condensed Matter—Proc. Int. Conf. on Condensed Matter under High Pressures* ed S K Sikka, S C Gupta and B K Godwal (New Delhi: National Institute of Science Communication) pp 12–9
[4] Brister K 1997 *Rev. Sci. Instrum.* **68** 1629–47
[5] Singh A K, Balasingh C, Mao H K, Hemley R J and Shu J 1998 *J. Appl. Phys.* **83** 7567–75
[6] Singh A K, Mao H K, Shu J and Hemley R J 1998 *Phys. Rev. Lett.* **80** 2157–60
[7] Mao H K, Shu J, Shen G, Hemley R J, Li B and Singh A K 1998 *Nature* **396** 741–3
Mao H K, Shu J, Shen G, Hemley R J, Li B and Singh A K 1999 *Nature* **399** 280 (correction)
[8] Stixrude L and Cohen R E 1995 *Science* **267** 1972–5
[9] Steinle-Neumann G, Stixrude L and Cohen R E 1999 *Phys. Rev.* B **60** 791–9
[10] Steinle-Neumann G, Stixrude L, Cohen R E and Gulseren O 2001 *Nature* **413** 57–60
[11] Duffy T S 2005 *Rep. Prog. Phys.* **68** 1811–59
[12] Duffy T S, Shen G, Heinz D L, Shu J, Ma Y, Mao H K, Hemley R J and Singh A K 1999 *Phys. Rev.* B **60** 15063–73
[13] Matthies S, Merkel S, Wenk H-R, Hemley R J and Mao H K 2001 *Earth Planet. Sci. Lett.* **194** 201–12
[14] Matthies S, Priesmeyer H G and Daymond M R 2001 *J. Appl. Crystallogr.* **34** 585–601
[15] Weidner D J, Li L, Davis M and Chen J 2004 *Geophys. Res. Lett.* **31** L06621
[16] Merkel S, Shu J, Gillet P, Mao H K and Hemley R J 2005 *J. Geophys. Res.* **110** B05201
[17] Wenk H-R, Matthies S, Hemley R J, Mao H K and Shu J 2000 *Nature* **405** 1044–7
[18] Kavner A 2003 *Earth Planet. Sci. Lett.* **214** 645–54
[19] Kavner A and Duffy T S 2001 *Geophys. Res. Lett.* **28** 2691–4
[20] Singh A K 1993 *J. Appl. Phys.* **73** 4278–86
Singh A K 1993 *J. Appl. Phys.* **74** 5920 (correction)
[21] He D, Shieh S R and Duffy T S 2004 *Phys. Rev.* B **70** 184121
[22] Merkel S, Jephcoat A P, Shu J, Mao H K, Gillet P and Hemley R J 2002 *Phys. Chem. Minerals* **29** 1–9
[23] Shieh S R, Duffy T S and Li B 2002 *Phys. Rev. Lett.* **89** 255507
[24] Duffy T S, Hemley R J and Mao H K 1995 *Phys. Rev. Lett.* **74** 1371–4
[25] Duffy T S, Shen G, Shu J, Mao H K, Hemley R J and Singh A K 1999 *J. Appl. Phys.* **86** 6729–36
[26] Kavner A and Duffy T S 2003 *Phys. Rev.* B **68** 144101
[27] Kiefer B, Shieh S R, Duffy T S and Sekine T 2005 *Phys. Rev.* B **72** 014102